

Fast multipole networks

Steve Huntsman¹

BAE Systems FAST Labs, 4301 North Fairfax Drive, Arlington, VA 22203, USA
 steve.huntsman@baesystems.com

Abstract. Two fundamental prerequisites for robotic multiagent systems are mobility and communication. We propose *fast multipole networks* (FMNs) to achieve both ends within a unified framework. FMNs can be organized very efficiently in a distributed way from local information and are ideally suited for motion planning using artificial potentials. We compare FMNs to conventional communication topologies, and find that FMNs offer favorable communication performance in addition to their intrinsic advantages for mobility.

Keywords: fast multipole method, network, random geometric graph, Delaunay triangulation, multirobot system, swarming

1 Introduction

A multirobot system [24] is a group of autonomous, networked robots. In order to achieve a complex goal such as swarming [8], the system requires distributed coordination of both mobility and communication. The respective enabling technologies are path planning and mobile *ad hoc* networks (MANETs) [28]. While networks are inevitably analyzed from the perspective of graph theory [3], path planning may be considered in either graph-theoretical [31] or continuous settings. Meanwhile, because geometrical considerations such as distance and motion strongly influence the structure of MANETs, it is natural to try to address mobility and communication for multirobot systems together. However, there has been little work to date in this direction apart from [40].

In this paper, we propose *fast multipole networks* (FMNs) to support both mobility and communication within a unified framework. The basic idea is to follow common practice in modeling robots, goals, and obstacles as (superpositions of) charged particles satisfying the Laplace equation $\nabla^2\phi = 0$ [9,22,35] and exploit the *fast multipole method* (FMM), an efficient algorithm for simulating particle dynamics [4,5,15], to simultaneously determine a sparse network topology that supports efficient communication. The animating principle that the far-field behavior of point charges [20] should determine a communication topology is geometrically natural. More surprisingly, we shall demonstrate that it leads to network topologies that perform well in their own right.

The overarching motivation is that multirobot systems will have nontrivial global, compositional, and emergent properties that respectively indicate analytical roles for (among other tools) topology [13], category theory [6,38], and

statistical physics [14]. FMNs implicitly draw on the second and third of these, and we outline these relationships in §A and §B, respectively. More generally, we anticipate that topological notions such as sheaves and simplicial sets, categorical notions such as symmetric monoidal categories and operads, and physical notions such as the free energy and the renormalization group will facilitate modeling and analyzing multirobot systems in a way that accounts for variation in platforms and their environments through carefully scoped parameters, interfaces, settings, etc. that not only respect but ultimately inform the organizational details necessary to engineer these systems effectively.

The paper is organized as follows. After briefly reviewing the artificial potential approach to path planning in §2 and the FMM in §3, we introduce FMNs in §4, and compare them to conventional MANET topologies in §5 before making concluding remarks in §6. Appendices §A and §B briefly discuss the FMM from the perspectives of category theory and statistical physics, respectively.

2 Artificial potentials

The use of artificial potentials in motion and path planning has a long history, most frequently identified as beginning with [21]. The basic idea is to design a potential ϕ such that the equation of motion $m\ddot{x} = -\nabla\phi$ results in a desired trajectory x . Towards this end, goals and obstacles are respectively modeled by attractive and repulsive terms contributing to the total potential ϕ . Depending on circumstances, we may choose to model the robots as “sources” with potentials of their own (e.g., to avoid collisions), or as passive “targets” that simply move along the gradient of an ambient potential.

In general, we might consider essentially arbitrary forms for each term to produce very detailed behavior. Alternatively, we might rely on a single simple form for all the terms. Our approach is in the latter vein. The relative strengths and spatial distribution of these terms are chosen to establish priorities, spatially extended features, etc. In order to represent sufficiently complex spatial relationships along these lines, it is helpful to have an algorithmic framework that scales better in total computational effort, parallelism, and locality than evaluating $O(N^2)$ interactions, since the number N of terms in the potential can be much larger than the number of robots involved.

Besides these computational concerns, a more pressing problem with using artificial potentials that was identified at an early stage is the possible presence of local minima in the potential field that can trap agents [23]. To remedy this problem by construction, the notion of a *navigation function* that has a single minimum at the goal was developed, along with algorithms for constructing such functions [37]. A particularly simple way to avoid metastable local minima while using a single form for all the potential terms is with a superposition of harmonic potentials [9,22,35], i.e., solutions to the Laplace equation $\nabla^2\phi = 0$, with a dominant term at the goal.

This is most readily achieved through a discrete (if perhaps quasi-continuous) superposition of *point charges*, i.e. potentials of the form $-qV(|x - x_0|)$ (the sign

is for physical reasons), where the *fundamental solution* $V(|x|)$ to the Laplace equation is defined by $\nabla^2 V(|x|) = \delta(x)$, and as usual δ indicates the Dirac delta distribution [41]. For \mathbb{R}^d , it turns out that $V'(r) = 1/A_d(r)$, where $A_d(r)$ is the Minkowski content (i.e., generalized surface area) of the sphere of radius r in \mathbb{R}^d . Choosing the most convenient constants of integration, for $d = 2$ we have $V(r) = \frac{1}{2\pi} \log r$, and for $d = 3$ we have $V(r) = -1/4\pi r$.

3 The fast multipole method

Naive simulation of N interacting point charges (e.g., the goals and obstacles modeled in Figure 1) requires computing the interactions of each pair of charges, and hence $O(N^2)$ operations per time step, which is prohibitive for large-scale N -body simulations. The FMM [4,5,15] enables the simulation cost to be reduced to $O(N)$ with an extremely high degree of locality and parallelism [16].¹

The key ideas underlying the FMM are

- i) a specification of accuracy (for truncating expansions in a controlled way);
- ii) decomposing space hierarchically to get *well-separated* charge clusters;²
- iii) representing well-separated clusters of point charges with multipole expansions that maintain a desired approximation error ε with as few ($\lceil \log_2(1/\varepsilon) \rceil$) terms as possible, leaving nearby particles to interact directly.

In particular, the FMM recursively builds a quad-tree (Figure 2; in three dimensions, an octo-tree is used instead) whose leaves are associated with boxes and truncated multipole expansions. This tree approximates a (typically much) finer tree whose leaves are associated with individual point charges that are well-separated and their monopoles. Importantly, the FMM tree topology essentially ignores the values of charges, depending only on the desired level of accuracy ε ³ and the locations of the charges.

The FMM can be fruitfully interpreted from the perspectives of category theory and/or statistical physics (via the renormalization group) along the respective lines of §A and §B, though we are not aware of discussions of either interpretation in the literature. §A is essentially a sketch of how the origins and coefficients of controlled series approximations to far-field potentials can be manipulated in a way analogous to the translation and scaling manifested in the little disks operad (Figure 9). The computationally expedient part of the FMM

¹ For the calculations in this paper, we used the very user-friendly library FMM-LIB2D, available at <https://cims.nyu.edu/cmcl/fmm2dlib/fmm2dlib.html>.

² This has a very specific meaning: two clusters of points $\{x_j\}$ and $\{y_k\}$ are well-separated iff there exist x_0, y_0 such that $\{x_j\} \subset B_{x_0}^\circ(r)$ and $\{y_k\} \subset B_{y_0}^\circ(r)$ with $|x_0 - y_0| > 3r$: here $^\circ$ denotes interior. Similarly, two squares with side length r are well-separated iff they are at distance $\geq r$.

³ Though in principle the desired level of accuracy can be affected by the values of charges (see, e.g., the error bounds in §A), this situation is sufficiently pathological that we can safely disregard it in practice.

is to focus these operations on clusters of point charges that are well-separated so that square boxes at regular locations can be considered instead of disks.

More general incarnations of the FMM (see, e.g., [26,43,44]) amount to a very efficient scheme for computing sums of the form $\sum_{j=1}^N K(x_i, \xi_j)\psi(\xi_j)$ for a given *kernel* K : i.e., the FMM and its generalizations are essentially specialized matrix multiplication algorithms. From this perspective, item iii) in the list above separates into [4]

- a far-field expansion of the kernel $K(x, \xi)$ that decouples the influence of the evaluation/target point x and the source point ξ ;
- (optionally) a conversion of far-field expansions into local ones (e.g., the Laurent-to-Taylor series conversion sketched in §A).

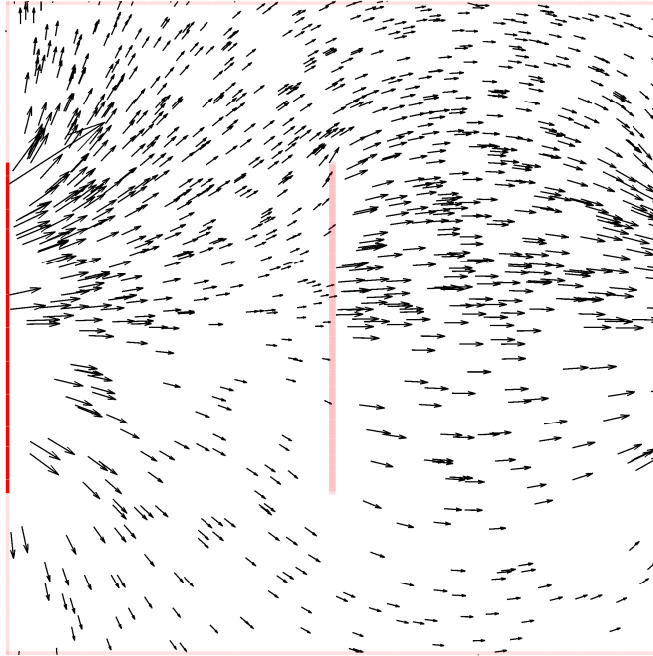


Fig. 1. A toy scenario in $[-1, 1]^2$. Goals are modeled by negative charges and shown in blue; obstacles are modeled by positive charges and shown in red. Opacity indicates the magnitude of charges. 10^3 robots are modeled by test points (versus, e.g., test charges of small positive sign) and their locations and velocities both indicated by black gradient vectors of the artificial potential. The target locations are distributed as $\frac{4}{5}U$ (top half) + $\frac{1}{5}U$ (bottom half), where here U indicates a uniform distribution.

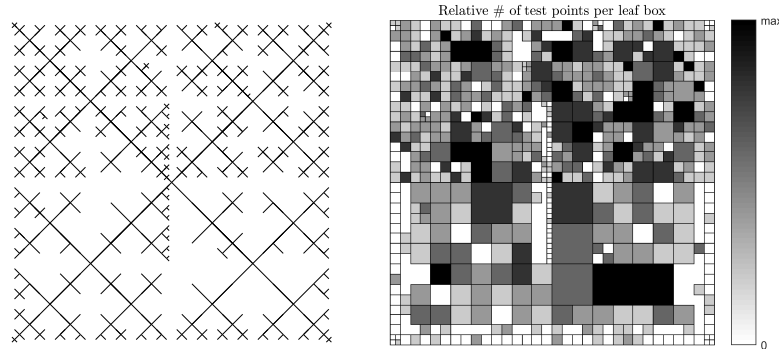


Fig. 2. (L) The quad-tree associated to the scenario in Figure 1. Varying the desired precision in the FMM has very little effect on this tree, and as a practical matter it can be assumed unique. (R) The associated spatial discretization, with relative number of test points indicated. Note that regions without test points do not have “leaf boxes.”

4 Fast multipole networks

The FMM’s remarkable scaling performance has enabled petascale simulations of turbulence [46], molecular dynamics [33], and cosmological dynamics [36], and will also enable future exascale simulations across hundreds of thousands of nodes [45]. This performance makes the FMM a natural choice for large scale path planning using artificial potentials.

Equally important for the considerations of this paper, however, are the hierarchical and spatial locality properties that the FMM exploits in order to communicate internally. The FMM’s patterning of a logical intra-algorithm communication network after the spatial distribution of particles suggests that it can be used not only for large-scale multirobot path planning in complex geometries, but also to help organize the communications between robots in a distributed way. Furthermore, although the FMM’s hierarchical properties might seem to imply centralization, the computational load is small enough that these functions can be easily duplicated among robots with low overhead.

We construct the *fast multipole network* $FMN(\xi)$ corresponding to a configuration of point charges at locations $\xi_j \in \mathbb{R}^2$ as follows: vertices correspond to the charge locations and we introduce edges that

- connect all vertices in the same FMM leaf box;
- connect nearest vertices in adjacent leaf boxes;
- connect otherwise isolated vertices to their nearest neighbors.

These three steps are respectively indicated by blue, cyan, and red edges in Figure 3.

By construction, $FMN(\xi)$ is connected, and the information required to generate it is automatically produced by the FMM. We note that while $FMN(\xi)$

is constructed using the quad- or octo-tree of the FMM, it is very far from a tree. Rather, the FMM tree and its corresponding coarse-graining of space determines which nodes are *permitted* to communicate directly.⁴ Within a clique of permitted communications corresponding to a leaf of the FMM tree, we may further restrict communications to avoid quadratic bandwidth overhead and/or energy, though we do not consider such tactics further here.

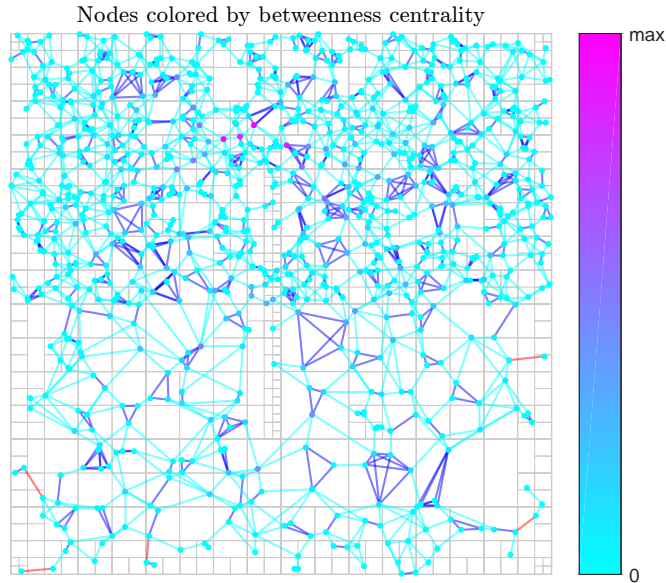


Fig. 3. The FMN corresponding to the scenario in Figure 1. Nodes are colored by betweenness centrality according to the colorbar on the right. The spatial decomposition from Figure 2 is shown in gray for reference. Edges within a FMM box are blue, while edges connecting nearest nodes in adjacent boxes are cyan and edges connecting otherwise isolated nodes to their nearest neighbors are red.

5 Evaluation

We now introduce several families of graphs for evaluation purposes.

Let $\xi_j \in \mathbb{R}^2$ for $1 \leq j \leq N$, and let $r > 0$. The *random geometric graph* (RGG; Figure 4) $RGG(\xi; r)$ has vertices ξ_j and edges $E(RGG(\xi; r)) := \{(\xi_j, \xi_k) : d(\xi_j, \xi_k) \leq r\}$ [18,34]. By construction, a RGG is both the most effective network

⁴ The limited permission for direct communication in FMNs may be usefully implemented by, e.g., cognitive radios [47] whose spectrum allocation algorithms work in concert with the FMM tree.

topology from the point of view of information exchange, and the least effective network topology from the point of view of infrastructure costs.

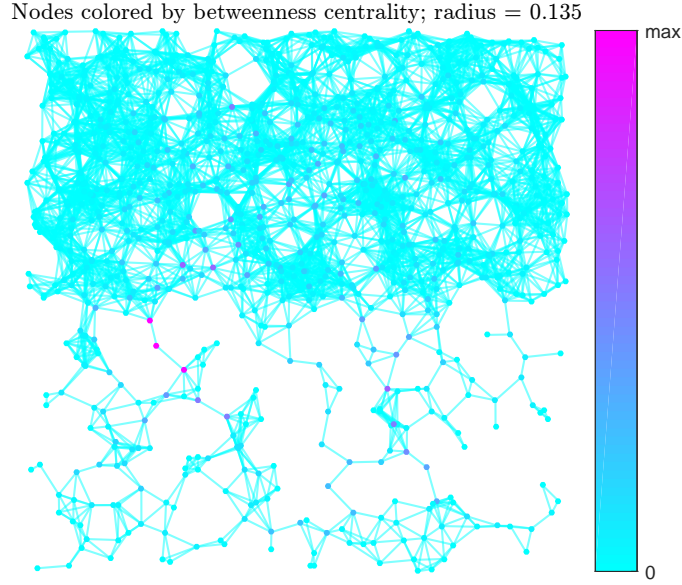


Fig. 4. $RGG(\xi; r)$ for ξ corresponding to the scenario in Figure 1 and $r = 0.135$, slightly above the threshold for connectivity.

A more conservative topology is based on subgraphs of the *Delaunay graph*. The Delaunay graph $D(\xi)$ has vertices ξ_j and edges defined from a triangulation of the vertices such that no vertex is interior to a circle circumscribed about a triangle [7,11,12].⁵ The *Gabriel graph* $G(\xi)$ [31,32] is the unique (for the general position case) subgraph of the Delaunay graph such that each edge corresponds to the diameter of a disk that does not contain any other vertices; it is frequently considered as a potential candidate for “virtual backbones” in MANETs. Because the Delaunay and Gabriel graphs do not have an intrinsic range parameter that will give a granular mechanism for evaluating their performance, we shall focus our attention on the (*minimal*) *restricted Delaunay graph* (Figure 5) $RD(\xi; r) := D(\xi) \cap RGG(\xi; r)$ [1] and the *restricted Gabriel graph* (Figure 6) $RG(\xi; r) := G(\xi) \cap RGG(\xi; r)$.

Similarly, we shall consider the *restricted FMN* (Figure 7) obtained along the lines $RFMN(\xi; r) := FMN(\xi) \cap RGG(\xi; r)$.

⁵ For ξ_j in general position, the Delaunay graph is unique.

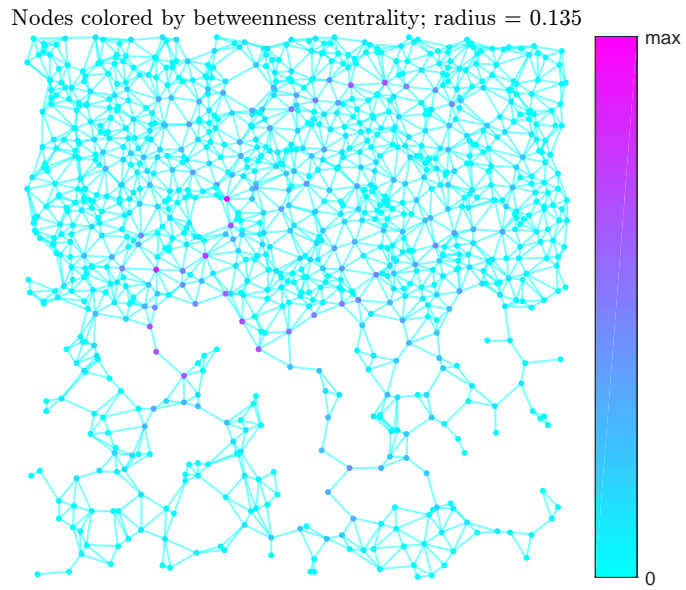


Fig. 5. $RD(\xi; r)$ for ξ corresponding to the scenario in Figure 1 and $r = 0.135$, slightly above the threshold for connectivity.

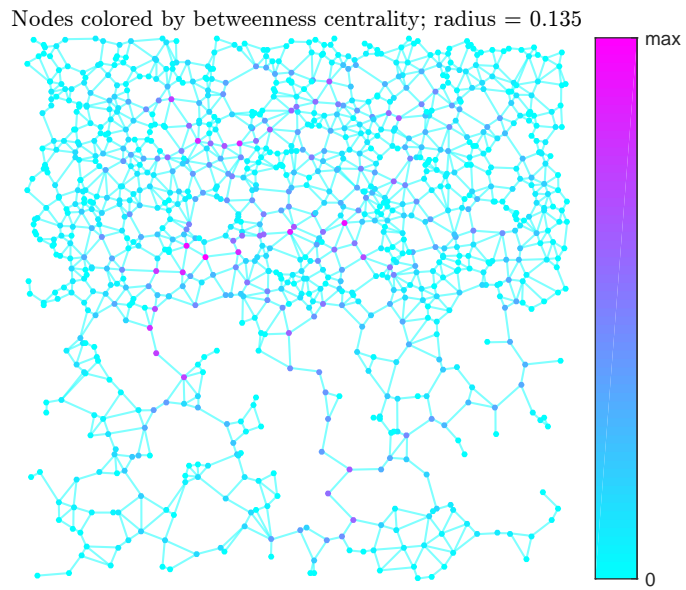


Fig. 6. $RG(\xi; r)$ for ξ corresponding to the scenario in Figure 1 and $r = 0.135$, slightly above the threshold for connectivity.

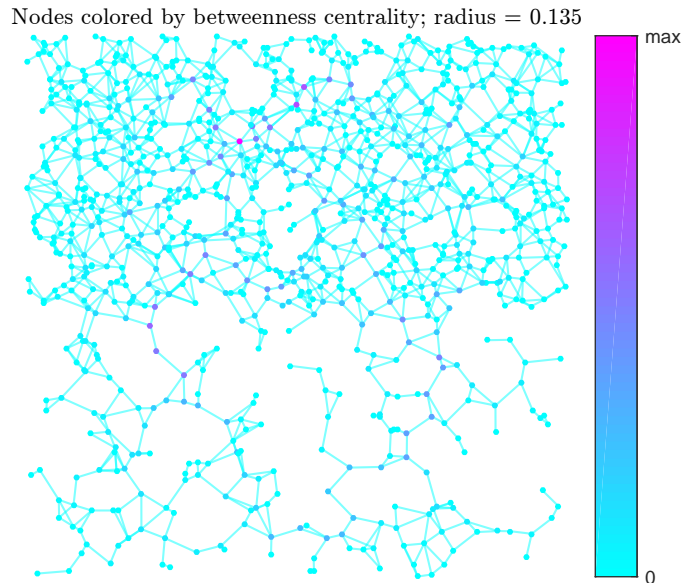


Fig. 7. $RFMN(\xi; r)$ for ξ corresponding to the scenario in Figure 1 and $r = 0.135$, slightly above the threshold for connectivity.

The basic evaluation metric we use is the *efficiency* of a graph $G = (V(G), E(G))$, defined as the average inverse distance between distinct vertices, i.e.

$$\text{eff}(G) := \binom{|V(G)|}{2}^{-1} \sum_{\substack{j, k \in V(G) \\ j \neq k}} \frac{1}{d_{jk}}, \quad (1)$$

where the distance d_{jk} between vertices j and k is computed in the obvious way from a given distance on edges (by default, we may always choose the *hop metric* that assigns 1 to each edge). While the efficiency characterizes how well a network supports information flow [25], it neglects any cost (e.g., bandwidth, energy, etc.) associated to edges as infrastructure. For this reason we will also consider the *efficiency per edge*, i.e. $\text{eff}(G)/|E(G)|$. Although other normalizations may be more appropriate in certain situations (e.g., normalizing by the sum of squared edge lengths for energy budgets), this particular one strikes a good balance between convenience/generalality and detail, especially for the hop metric.

Figure 8 shows the metrics above for 100 simulations of 10^3 uniformly distributed test points in $[-1, 1]^2$ subject to the ambient potential from Figure 1. It is apparent from the figure that FMNs and their range-restricted versions are worthy candidates for network backbones in their own right even before accounting for their mobility-specific advantages. Furthermore, although there exist efficient local and parallel algorithms for constructing Delaunay graphs [7,11,12],

their computation and communication complexity and scaling behavior are still inferior to the FMM.

6 Remarks

By virtue of calculating potentials and forces, the FMM/FMN approach enables dynamic and predictable network topology reconfiguration with minimal cost and effort. Incorporating a generalization of the resilient routing reconfiguration [42] suitable for wireless networks (i.e., with point-to-multipoint links) [10] on $(F + 1)$ -connected local subgraphs of the FMN can be done with reasonable computational effort (e.g., the key linear program is quickly and easily solved in MATLAB for realistic networks of ≈ 50 nodes). This enables virtually instantaneous failover and rerouting in the presence of $\leq F$ link failures.

Combining this local approach with a separate (perhaps similar) routing protocol to handle wide-area network traffic and obstacle potentials that prevent deterioration of basic connectivity can ensure network integrity and basic quality of service (QoS). These features can render our framework competitive with the approach of [40], which centers on the higher-level functions of network integrity and QoS, and which uses a convex program instead of an algorithmically simpler linear program.

It is worth pointing out that there are FMM variants for non-harmonic potentials, e.g. power laws, (generalized) multiquadrics [4,44], or more general kernels [26], and many of these have actually been applied in the context of interpolation and/or physical simulation. However, using non-harmonic potentials eliminates the automatic guarantee that there are no metastable local minima. We note in particular that the kernel-independent FMM variant of [43] exploits the existence and uniqueness of solutions to elliptic boundary value problems [41] to represent clustered sources in far field based on their behavior on a suitable boundary. This perspective suggests not only an extension of FMNs to sources modeled by fundamental solutions of elliptic PDEs, but also a concomitant generalization of the fast multipole operad of §A.

A The fast multipole operad

From the point of view of category theory, it can be helpful to think of the FMM as leveraging an *operad* [27,29,39] of configurations of point charges. At a high level, an operad is a collection of objects that “plug into each other” like maps of the form $f_{(m)} : X^m \rightarrow X$ à la

$$f_{(m)} \circ_{\ell} g_{(n)} := f(\cdot_1, \dots, \cdot_{\ell-1}, g(\cdot_{\ell}, \dots, \cdot_{\ell+n-1}), \cdot_{\ell+n}, \dots, \cdot_{m+n}).$$

This somewhat obscure formulation encodes essential features of the FMM and abstracts away the analytical details of multipole expansions in a way that we outline below. In particular, it codifies that the FMM aggregates multipole expansions that correspond to clusters of point charges, and vastly generalizes the

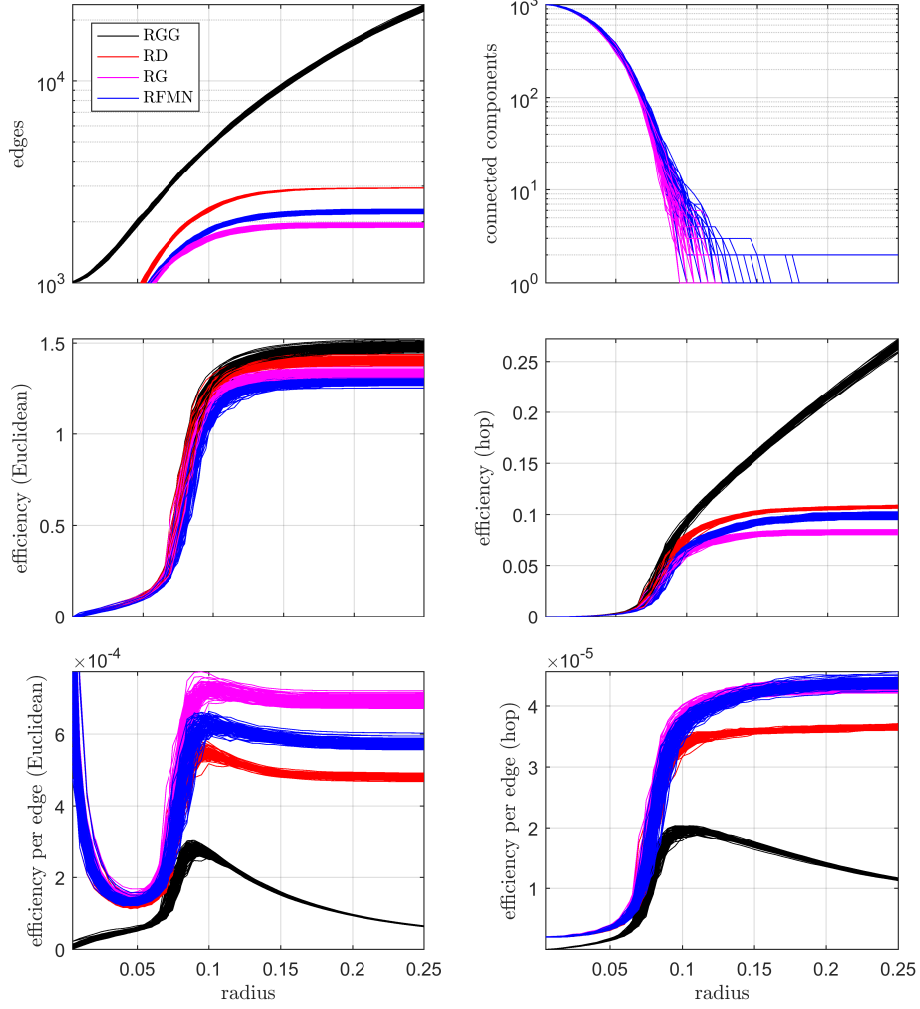


Fig. 8. Network metrics for $RGG(\xi; r)$ (in black), $RD(\xi; r)$ (in red), $RG(\xi; r)$ (in magenta), and $RFMN(\xi; r)$ (in blue) for 100 simulations of $N = 10^3$ uniformly distributed test charges in $[-1, 1]^2$. Although $RGG(\xi; r)$ is most efficient, this network performance comes at a high cost in edges, and $RFMN(\xi; r)$ performs well (and for hop efficiency per edge, the best) for all measures of efficiency. Note that $RFMN(\xi; r) = FMN(\xi)$ for sufficiently large r within the range shown. We also have that, e.g. $RD(\xi; r') = D(\xi)$, and though the corresponding r' is outside the range shown, the residual effects are minimal.

observation that a cluster of point charges can be approximated (up to higher-order moments that are irrelevant in the far-field regime) by a single point charge.

While the details for signed charges are intricate, a “gravitational” case is straightforward to sketch (though its formalization would still involve considerable effort). The intuition underlying this “monopole operad” is that in the far-field regime, many point masses behave like a single point mass. The details involve a synthesis of a weighted little disks operad that accounts for the nesting of point mass clusters and normalized masses (Figure 9), along with the fundamental solution $V(|x|)$ to the Laplace equation. Given point masses $m_j > 0$ at

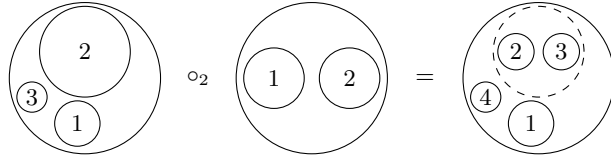


Fig. 9. Composition in the little disks operad. In a weighted variant, if the little disks in the first and second arguments on the LHS have respective weight tuples (m_1, m_2, m_3) and (m'_1, m'_2) , then the little disks on the RHS have weight tuple $(m_1, m_2 m'_1 / (m'_1 + m'_2), m_2 m'_2 / (m'_1 + m'_2), m_3)$.

locations $\xi_j \in \mathbb{R}^d$, superpositions of the form

$$V_{\xi, m}(x) := \sum_j m_j V(|x - \xi_j|) \sim \sum_j m_j V(|x|)$$

are endowed with an operadic composition along the lines of

$$V_{\xi, m} \circ (V_{\xi^{(1)}, m^{(1)}}, \dots, V_{\xi^{(n)}, m^{(n)}})(x) := \sum_j \frac{m_j}{|m^{(j)}|} V_{\xi^{(j)}, m^{(j)}}(x - \xi_j) \sim V_{\xi, m}(x).$$

To sketch the picture for signed charges, first write for $a_k, z \in \mathbb{C}$

$$\mu(z; a_0, \dots, a_p) := a_0 \log z + \sum_{k=1}^p \frac{a_k}{z^k}. \quad (2)$$

The multipole expansion gives a controlled approximation to the far-field behavior of a configuration of point charges. Using the complex variable z in two dimensions (and implicitly taking real parts of potentials to get physically meaningful results) for convenience, the potential $-V_{\xi, q}(z)$ produced by n point charges q_j at locations $\xi_j \in B_r(0) \subset \mathbb{C}$ obeys the error estimate

$$|-V_{\xi, q}(z) - \mu(z; a_0, \dots, a_p)| \leq \frac{A}{1 - \frac{r}{|z|}} \left| \frac{r}{z} \right|^{p+1}, \quad (3)$$

for $z \notin B_r(0)$, where $a_0 := \sum_{j=1}^n q_j$, $a_k := -\frac{1}{k} \sum_{j=1}^n q_j \xi_j^k$ for $k > 0$, and $A := \sum_{j=1}^n |q_j|$. In particular, $-V_{\xi, q}(z) = \mu(z; a_0, \dots)$ for $z \notin B_r(0)$.

If instead the point charges are in $B_r(\xi_0)$, we can shift the origin of the multipole expansion using

$$|\mu(z - \xi_0; a_0, \dots) - \mu(z; a_0, b_1, \dots, b_p)| \leq \frac{A}{1 - \left| \frac{r + |\xi_0|}{z} \right|} \left| \frac{r + |\xi_0|}{z} \right|^{p+1}, \quad (4)$$

for $z \notin B_{r+|\xi_0|}(0)$, and for certain coefficients b_ℓ that are readily computable in closed form. If furthermore $|\xi_0| > (c+1)r$ for some $c > 1$ and $p \geq 2 \max\{1, \frac{c}{c-1}\}$, then for $z' \in B_r(0)$ we have a Taylor expansion:

$$\left| \mu(z - \xi_0; a_0, \dots) - \sum_{\ell=0}^p b'_\ell z'^\ell \right| < \frac{A(4e(p+c)(c+1) + c^2)}{c(c-1)} c^{-(p+1)}, \quad (5)$$

where again the b'_ℓ have a readily computable closed form. Note that it is trivial to shift the origin of this Taylor expansion using the binomial theorem.

Again, the error bounds (3)-(5) allow us to efficiently approximate the interactions of clusters of point charges that are bounded by well-separated disks, and the FMM rests on manipulating these error bounds in a way that generalizes the little disk and monopole operads in concert with a computationally convenient multiresolution grid.

Finally, we remark that operadic formulations or realizations of data structures for multirobot systems such as the one sketched here are especially desirable because they hold the promise of engineering distinct functionalities in a coherent way. For example, detailed missions can be encoded using flowgraphs [19], constraints can be encoded using weighted maximum satisfiability and/or linear temporal logic formulas, teams can be encoded using simplicial sets [17], etc., and each of these data structures has an associated notion of operad.

B The renormalization group

The *renormalization group* [2,14,30] is a perspective on coarse-graining and scaling behavior in physical systems. At a high level, we consider a theory given by a function $f(x; \theta)$ of data x and parameters θ . If for a suitable coarse-graining operator C there exists a function g such that $f(C(x); g(\theta))$, then the theory is renormalizable.⁶ The fixed point of this renormalization group transformation for infinite domains is of great physical interest, as it describes thermodynamically critical points.⁷

For the monopole operad described in §A, we can take f to be a superposition of potential fields; x is the set of particle locations; $\theta = m$ are “masses” (or

⁶ The fact that general relativity is not renormalizable is the principal obstruction to a theory of quantum gravity.

⁷ Amusingly, there is a renormalization interpretation of the Debye-Hückel theory for “gases” of opposing point charges with equal density [30]. The physical idea is that a constant “bare charge” is replaced with a renormalized or “screened” charge whose effective strength decays exponentially with distance.

charges of the same sign), C clusters particle locations, and g aggregates masses in a way suggested by Figure 9.

Acknowledgements

We thank BAE Systems FAST Labs for its support, and Brendan Fong, Marco Pravia, and David Spivak for useful conversations.

References

1. Avin, C. “Fast and efficient restricted Delaunay triangulation in random geometric graphs.” *Internet Math.* **5**, 195 (2008).
2. Barenblatt, G. I. *Scaling*. Cambridge (2003).
3. Barrat, A., Barthélemy, M., and Vespignani, A. *Dynamical Processes on Complex Networks*. Cambridge (2008).
4. Beatson, R. and Greengard, L. “A short course on fast multipole methods.” In *Wavelets, Multilevel Methods, and Elliptic PDEs*. Ainsworth, M., *et al.*, eds. Oxford (1997).
5. Board, J. and Schulten, L. “The fast multipole algorithm.” *Comp. Sci. Eng.* **2**, 76 (2000).
6. Breiner, S., Subrahmanian, E., and Jones, A. “Categorical foundations for system engineering.” CSER (2018).
7. Chen, R. and Gotsman, C. “Localizing the Delaunay triangulation and its parallel implementation.” ISVD (2012).
8. Chung, S.-J., *et al.* “A survey on aerial swarm robotics.” *IEEE Trans. Robotics* **34**, 837 (2018).
9. Connolly, C. I., Burns, J. B. and Weiss, R. “Path planning using Laplace’s equation.” ICRA (1990).
10. DeCleene, B. and Huntsman, S. “Wireless resilient routing reconfiguration.” Preprint (2019).
11. Fuetterling, V., Lojewski, C., and Pfreundt, F.-J. “High-performance d -D Delaunay triangulations for many-core computers.” HPG (2014).
12. Funke, D. and Sanders, P. “Parallel d -D Delaunay triangulations in shared and distributed memory.” ALNEX (2017).
13. Ghrist, R. *Elementary Applied Topology*. Createspace (2014).
14. Goldenfeld, N. *Lectures on Phase Transitions and the Renormalization Group*. Addison-Wesley (1992).
15. Greengard, L. and Rokhlin, V. “A fast algorithm for particle simulations.” *J. Comp. Phys.* **73**, 325 (1987).
16. Greengard, L. and Gropp, W. D. “A parallel version of the fast multipole method.” *Comp. Math. Appl.* **20**, 63 (1990).
17. Greening, B. R., Pinter-Wollman, N., and Fefferman, N. H. “Higher-order interactions: understanding the knowledge capacity of social groups using simplicial sets.” *Curr. Zool.* **61**, 114 (2015).
18. Haenggi, M. *Stochastic Geometry for Wireless Networks*. Cambridge (2013).
19. Huntsman, S. “The multiresolution analysis of flow graphs.” arXiv.org:1701.07051 (2017).
20. Jackson, J. D. *Classical Electrodynamics*. 3rd ed. Wiley (1998).

21. Khatib, O. "Real-time obstacle avoidance for manipulators and mobile robots." ICRA (1985).
22. Kim, J.-O. and Khosla, P. K. "Real-time obstacle avoidance using harmonic potential functions." *IEEE Trans. Robotics and Automation* **8**, 501 (1992).
23. Koren, Y. and Borenstein, J. "Potential field method and their inherent limitations for mobile robot navigation." ICRA (1991).
24. Knorn, S., Chen, Z., and Middleton, R. H. "Overview: collective control of multi-agent systems." *IEEE Trans. Cont. Net. Sys.* **3**, 334 (2016).
25. Latora, V. and Marchiori, M. "Efficient behavior of small-world networks." *Phys. Rev. Lett.* **87**, 198701 (2001).
26. Létourneau, P.-D., Cecka, C., and Darve, E. "Cauchy fast multipole method for general analytic kernels." *SIAM J. Sci. Comp.* **36**, A396 (2014).
27. Leinster, T. *Higher Operads, Higher Categories*. Cambridge (2004).
28. Loo, J., Mauri, J. L., and Ortiz, J. H., eds. *Mobile Ad Hoc Networks*. CRC (2016).
29. Markl, M., Shnider, S., and Stasheff, J. *Operads in Algebra, Topology, and Physics*. AMS (2007).
30. McComb, W. D. *Renormalization Methods: A Guide for Beginners*. Oxford (2004).
31. Mesbahi, M. and Egerstedt, M. *Graph Theoretic Methods in Multiagent Networks*. Princeton (2010).
32. Norrenbrock, C. "Percolation threshold on planar Euclidean Gabriel graphs." *Eur. Phys. J. B* **89**, 111 (2016).
33. Ohno, Y., *et al.* "Petascale molecular dynamics simulation using the fast multipole method on K computer." *Comp. Phys. Comm.* **185**, 2575 (2014).
34. Penrose, M. *Random Geometric Graphs*. Oxford (2003).
35. Pimenta, L. C. A., *et al.* "On computing complex navigation functions." ICRA (2005).
36. Potter, D., Stadel, J., and Teyssier, R. "PKDGRAV3: beyond trillion particle cosmological simulations for the next era of galaxy surveys." *Comp. Astrophys. Cosmol.* **4**, 2 (2017).
37. Rimon, E. and Koditschek, D. E. "Exact robot navigation using artificial potential functions." *IEEE Trans. Robotics and Automation* **8**, 501 (1992).
38. Spivak, D. I. *Category Theory for the Sciences*. MIT (2014).
39. Stasheff, J. "What is an operad?" *Not. AMS* **51**, 630 (2004).
40. Stephan, J., *et al.* "Concurrent control of mobility and communication in multi-robot systems." *IEEE Trans. Robotics* **33**, 1248 (2017).
41. Taylor, M. E. *Partial Differential Equations: Basic Theory*. Springer (1996).
42. Wang, Y. *et al.* "R3: resilient routing reconfiguration." SIGCOMM (2010).
43. Ying, L., Biros, G., and Zorin, D. "A kernel-independent adaptive fast multipole algorithm in two and three dimensions." *J. Comp. Phys.* **196**, 591 (2004).
44. Ying, L. "A kernel-independent fast multipole algorithm for radial basis functions." *J. Comp. Phys.* **213**, 457 (2006).
45. Yokota, R. and Barba, L. A. "A tuned and scalable fast multipole method as a preeminent algorithm for exascale systems." *Int. J. High Perf. Comp. Appl.* **26**, 337 (2012).
46. Yokota, R., *et al.* "Petascale turbulence simulation using a highly parallel fast multipole method on GPUs." *Comp. Phys. Comm.* **184**, 445 (2013).
47. Yu, R. F., ed. *Cognitive Radio Mobile Ad Hoc Networks*. Springer (2011).